Polyene Cyclization by a Double Intramolecular Heck Reaction. A DFT Study

David Balcells,[†] Feliu Maseras,[†] Brian A. Keay,[‡] and Tom Ziegler*,[‡]

Unitat de Química Física, Edifici Cn, Universitat Autònoma de Barcelona, 08193 Bellaterra, Catalonia, Spain, and Department of Chemistry, University of Calgary, 2500 University Drive NW, Calgary, Alberta, Canada T2N 1N4

Received November 19, 2003

A density functional theory (DFT) model study has been carried out on the cyclization of aryl polyene triflate catalyzed by a Pd(II)-BINAP complex in a Heck type reaction. In the model study, the catalyst was represented by $Pd(PH_2(CH)_4PH_2)$, whereas the aryl polyene triflate substrate was simplified by replacing the dimethoxy naphthalene fragment with hydrogens. Formally, this cyclization reaction consists of an intramolecular Heck reaction with two olefin insertions, also known as a double or cascade Heck reaction. The postulated cationic pathway for aryl triflate substrates has been explored as the reaction mechanism. The study has mainly focused on the two migratory insertion steps, where the identity of the final reaction products is decided. At both steps two distinct insertions may occur: exo, or 1,2-insertion, and endo, or 2,1-insertion. The computation of the possible intermediates and transition states demonstrated that the first insertion is exo-selective, with an energy barrier of only 4.1 kcal/mol, while the second insertion is endo-selective, involving a much higher energy barrier of 22.8 kcal/mol. The calculated subsequent preference for exo and endo selectivity is in good agreement with qualitative experimental observation. According to our results, the main factor controlling the exo/endo selectivity, at both the thermodynamic and the kinetic levels, is the relative stability of the cyclic system resulting from the migratory insertion. Furthermore, a furan ring present in the substrate can play an important role by forming a stable and inert π-complex that is able to suppress subsequent migratory insertion steps. On the other hand, taking into account the solvent effects using a continuum model, we found that the exo/endo selectivity of the first insertion step is solvent-dependent. As the polarity of the solvent increases, the relative stability of the endo intermediate also increases, in good agreement with the available experimental data. The β-elimination steps affording the final reaction products were also investigated. The results show that the β-elimination on the endo intermediates is thermodynamically favored over the β-elimination on the exo intermediates. On the other hand, the results for the β-elimination on the endo intermediates show that this reaction is highly reversible.

Introduction

The C−C bond formation by means of the Heck reaction (Scheme 1) is one of the most versatile and important palladium-catalyzed transformations in organic chemistry.[1−10] The Heck reaction can be performed in both intramolecular and intermolecular fashions, and in many cases, depending on the identity of the substrate, different regioisomers and/or diastereoisomers and/or enantiomers can be formed. Hence, a

Scheme 1. Heck Reaction (top) and Its "Textbook" Reaction Mechanism (bottom)

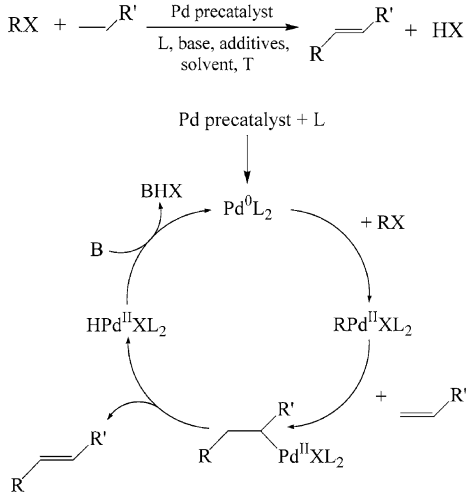

[†] Universitat Autònoma de Barcelona.
[‡] University of Calgary.

(1) Heck, R. F. In *Comprehensive Organic Synthesis*; Trost, B. M., Fleming, I., Eds.; Pergamon Press: Oxford, 1991; Vol. 4.
(2) Daves, G. D.; Hallberg, A. *Chem. Rev.* **1989**, *89*, 1433.
(3) De Meijere, A.; Meyer, F. E. *Angew. Chem., Int. Ed. Engl.* **1995**, *33*, 2379.
(4) Braese, S.; De Meijere, A. In *Metal-Catalyzed Cross-Coupling Reactions*; Diederich, F., Stang, P. J., Eds.; Wiley-VCH: New York, 1998.
(5) Cabri, W.; Candiani, I. *Acc. Chem. Res.* **1995**, *28*, 2.
(6) Crisp, G. T. *Chem. Soc. Rev.* **1998**, *27*, 427.
(7) Beletskaya, I. P.; Cheprakov, A. V. *Chem. Rev.* **2000**, *100*, 3009.
(8) Herrmann, W. A. In *Applied Homogeneous Catalysis with Organometallic Compounds*; Cornils, B., Herrmann, W. A., Eds.; Wiley-VCH: New York, 2002.
(9) Dounay, A. B.; Overman, L. E. *Chem. Rev.* **2003**, *103*, 2945.
(10) Shibasaki, M.; Vogl, E. M. *J. Organomet. Chem.* **1999**, *576*, 1.

10.1021/om034310c CCC: $27.50
Publication on Web 04/22/2004

mechanistic understanding of the reaction is required in order to obtain selectively the desired reaction products.

The general and widely accepted $Pd^{0/II}$ mechanism for the Heck reaction is depicted in Scheme 1. An alternative reaction pathway involving a $Pd^{II/IV}$ redox cycle has been proposed[11] as well. However, a recent theoretical study by Martin et al. has demonstrated that this reaction mechanism is feasible only if a weakly coordinating ligand is present.[12] The mechanistic picture in Scheme 1 collects all the elementary steps involved in the Heck reaction. Depending on the nature of the catalyst and the substrate, recent experimental[7,9,13−23] and theoretical studies[23−26] have added further complexity to the general mechanism shown in Scheme 1. Thus, pathways with cationic as well as neutral and anionic active species have been postulated for different experimental systems. The main difference between the neutral and cationic paths is that in the former case X = OTf/halide (OTf = $-OSO_2CF_3$, triflate) is bound to palladium, while in the latter it is outside the first coordination sphere of the metal. The cationic path has been assigned to X = OTf,[13−17] while the neutral path seems to play an important role when X = halide.[18−20] This difference at the mechanistic level has been used to explain why the reactivities and enantioselectivities of the Heck reactions involving OTf and halides are completely different. Finally, some experimental studies by Amatore et al. suggest that when $Pd(OAc)_2$ is used as precatalyst, the active species is an anionic palladium complex.[21,22]

During the past decade, the asymmetric intramolecular Heck reaction has emerged as a powerful tool in natural product synthesis.[9] The total synthesis of different biologically active terpenoids,[27−30] alkaloids,[31−34] and polyketides[35−37] has been achieved using the asymmetric intramolecular Heck reaction as the key synthetic step. We shall here study the challenging total synthesis of (+)-xestoquinone carried out by Keay et al.[36] as an interesting application of the Heck reaction; see Scheme 2. In this case, the Heck reaction is used to perform the asymmetric cyclization of the aryl polyene triflate **A**, yielding the optically active polycyclic ketone **I**. A feasible reaction mechanism for this catalytic system, assuming the cationic path postulated for the aryl triflate substrates, involves an initial oxidative addition of the substrate **A** to the catalyst, affording the cationic aryl palladium(II) complex **B**; see Scheme 3. At this step we find the first branching point along the reaction pathway, due to the two possible ways in which the olefin insertion may proceed. The first (exo) path yields a six-membered ring (**C**), while the second (endo) path gives rise to the formation of a seven-membered ring (**D**). Hence these pathways are labeled as 6-exo and 7-endo, respectively. At the next stage of the reaction mechanism two outcomes are possible: a β-elimination in **D** yielding the endo reaction product **E** or a second olefin insertion involving either **C** or **D**. In the latter case, the Heck reaction is referred to as a cascade or double (insertion) reaction. The second migratory insertion can give rise to both a exo and a endo route. The possible pathways, taking into account the size of the formed rings, are 5-exo (**F**) and 6-endo (**G**), starting from the 6-exo alkyl palladium(II) complex **C**, and 4-exo (**J**) and 5-endo (**K**), starting from the 7-endo alkyl palladium(II) complex **D**. A β-elimination in the resulting alky palladium(II) complexes **F** and **G** leads finally to the formation of the reaction products **H** and **I**, while **J** and **K** transform to **L** and **M**. Hence, the reaction could potentially afford five different products (**E**, **H**, **I**, **L**, **M**), Scheme 3. Nevertheless, the experimental results show that the unsaturated polycyclic ketone **I**, resulting from

Scheme 2. Last Steps of the Total Synthesis of (+)-Xestoquinone

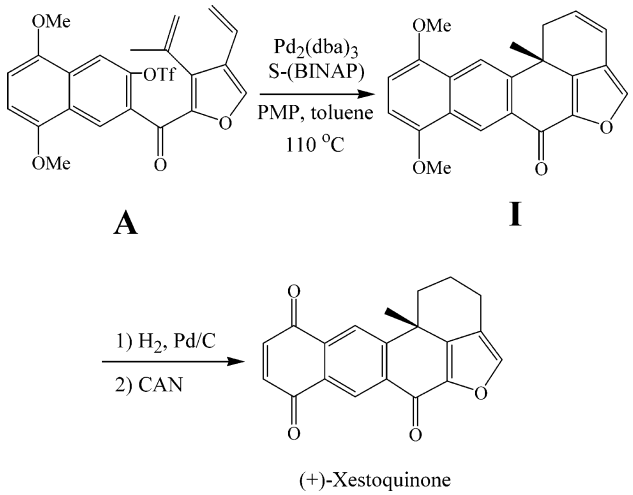

(11) Shaw, B. L. *New J. Chem.* **1998**, 77.
(12) Sundermann, A.; Uzan, O.; Martin, J. M. L. *Chem. Eur. J.* **2001**, *7*, 1703.
(13) Amatore, C.; Jutand, A. *J. Organomet. Chem.* **1999**, 254.
(14) Cabri, W.; Candiani, I.; DeBernardis, S.; Francalanci, F.; Penco, S. *J. Org. Chem.* **1991**, *56*, 5796.
(15) Ozawa, F.; Kubo, A.; Hayashi, T. *J. Am. Chem. Soc.* **1991**, *113*, 1417.
(16) Jutand, A.; Négri, S. *Organometallics* **2003**, ASAP.
(17) Alcazar-Roman, L. M.; Hartwig, J. F. *Organometallics* **2002**, *21*, 491.
(18) Ashimori, A.; Overman, L. E. *J. Org. Chem.* **1992**, *57*, 4571.
(19) Overman, L. E.; Poon, D. J. *Angew. Chem., Int. Ed. Engl.* **1997**, *36*, 518.
(20) Jutand, A.; Hii K. K.; Thornton-Pett, M.; Brown, J. M. *Organometallics* **1999**, *18*, 5367.
(21) Amatore, C.; Jutand, A. *Acc. Chem. Res.* **2000**, *33*, 314.
(22) Amatore, C.; Carré, E.; Jutand, A.; M'Barki, M. *Organometallics* **1995**, *14*, 5605.
(23) Hii, K. K.; Claridge, T. D. W.; Brown, J. M.; Smith, A.; Deeth, R. J. *Helv. Chim. Acta* **2001**, *84*, 3043.
(24) Albert, K.; Gisdakis, P.; Rösch, N. *Organometallics* **1998**, *17*, 1608.
(25) Schenck, H.; Åkermark, B.; Svensson, M. *J. Am. Chem. Soc.* **2003**, *125*, 3503.
(26) Schenck, H.; Åkermark, B.; Svensson, M. *Organometallics* **2002**, *21*, 2248.
(27) Ohrai, K.; Kondo, K.; Sodeoka, M.; Shibasaki, M. *J. Am. Chem. Soc.* **1994**, *116*, 11737.
(28) Sato, Y.; Mori, M.; Shibasaki, M. *Tetrahedron: Asymmetry* **1995**, *6*, 757.
(29) Tietze, L. F.; Rashke, T. *Synlett.* **1995**, 597.
(30) Ohshima, T.; Kagechika, K.; Adachi, M.; Sodeoka, M.; Shibasaki, M. *J. Am. Chem. Soc.* **1996**, *118*, 7108.
(31) Ashimori, A.; Bachand, B.; Overman, L. E.; Poon, D. J. *J. Am. Chem. Soc.* **1998**, *120*, 6477.
(32) Nukui, S.; Sodeoka, M.; Sasai, H.; Shibasaki, M. *J. Org. Chem.* **1995**, *60*, 398.
(33) Kiewel, K.; Tallant, M.; Sulikowski, G. A. *Tetrahedron Lett.* **2001**, *42*, 6621.
(34) Yoda, H.; Katoh, H.; Ujihara, Y.; Takabe, K. *Tetrahedron Lett.* **2001**, *42*, 2509.
(35) Kojima, A.; Takemoto, T.; Sodeoka, M.; Shibasaki, M. *Synthesis* **1998**, 581.
(36) Maddaford, S. P.; Andersen, N. G.; Cristofoli, W. A.; Keay, B. A. *J. Am. Chem. Soc.* **1996**, *118*, 10766. (b) Miyazaki, F.; Uotso, K.; Shibasaki, M. *Tetrahedron* **1998**, *54*, 13073.
(37) Mizutani, T.; Honzawa, S.; Tosaki, S. Y.; Shibasaki, M. *Angew. Chem., Int. Ed.* **2002**, *41*, 4680.

Scheme 3. Possible Reaction Pathways in the Cationic Double-Insertion Mechanism

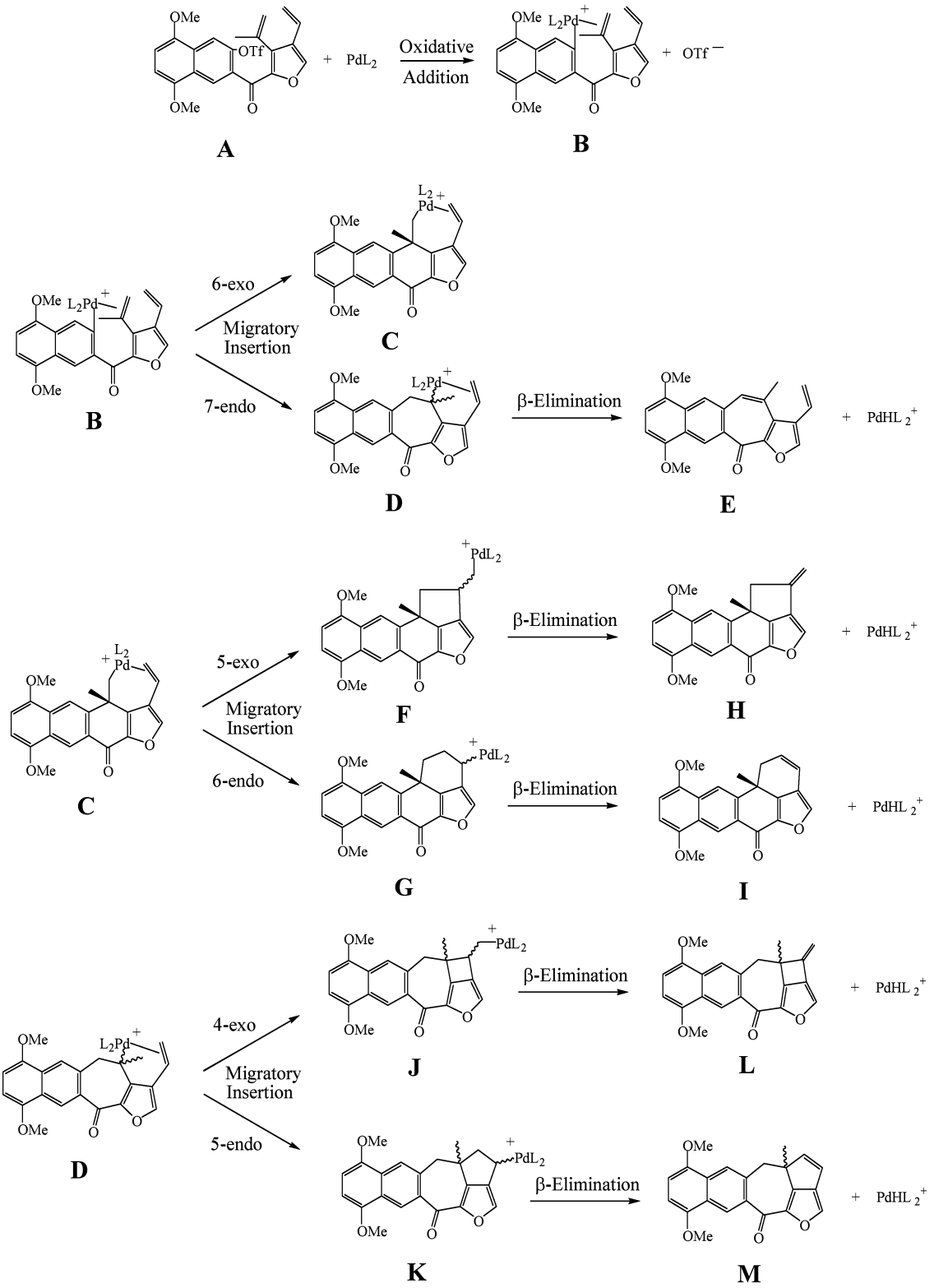

a double olefin insertion, is always obtained as the main reaction product. In fact, one of the most interesting aspects of this reaction is the change in the exo/endo regioselectivity from 6-exo in the first insertion to 6-endo in the second. On the other hand, a 2.5:1 mixture of the **I** and **E** products was observed when NMP (*N*-methyl-2-pyrrolidone) was used as solvent instead of toluene. We shall in the following try to understand the factors determining the observed product distribution by determining the relative stabilities of the reaction intermediates formed along the reaction pathway as well as the energy barriers of the involved elementary reaction steps.

During the past decade, computational chemistry has emerged as a suitable method for the elucidation of reaction mechanisms in homogeneous catalysis.[38−40] Previous theoretical studies on the Heck reaction have focused on the common intermolecular single olefin

Scheme 4. Modelization of the Catalytic System

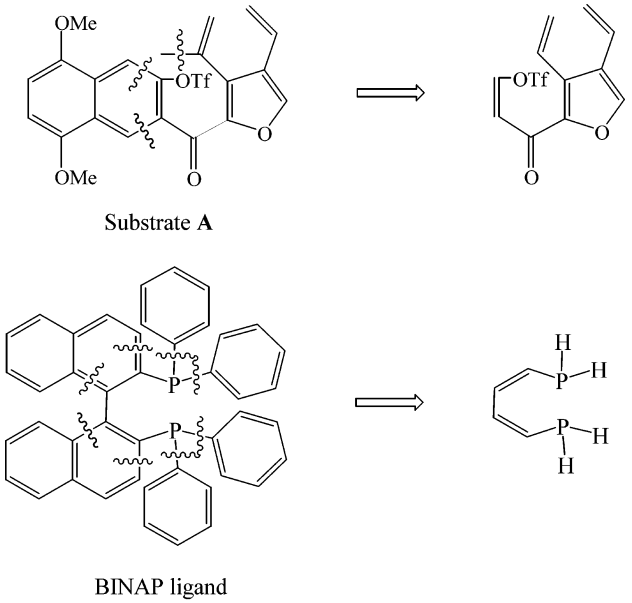

insertion variant of the reaction.[12,23−26] Thus, the main scope of the present theoretical study is to provide the first detailed mechanistic description of an intramolecular double Heck reaction.

System Modeling and Computational Details

The real catalytic system (see Scheme 2) is too large for a full quantum chemical investigation of all the possible reaction paths at a level of suitable accuracy. Because of this, we decided to simplify the system as shown in Scheme 4. On the BINAP ligand, all the aromatic rings were eliminated without breaking the conection between the two basic phosphorus atoms. Thus, the basic bidentate character of the ligand was maintained. In the substrate, the dimethoxy naphthalene fragment was eliminated as well as the methyl attached to one of the olefins. All the eliminated fragments were replaced by hydrogen atoms in order to avoid dangling bonds. On the basis of previous experimental investigations[13−17] we assume that OTf^- is completely dissociated from the Pd-catalyst.

We are aware that this structural simplification in both catalyst (ligand) and substrate molecules will completely eliminate the enantioselectivity of the reaction. However, we think that the resulting model accounts for the main electronic effects driving the catalytic cycle and, therefore, is capable of providing a meaningful description of the reaction mechanism. The molecular fragments missing in our model are likely to play mainly a steric role by inducing the observed enantioselectivity. This aspect will be studied later by making use of the QM/MM methodology, where quantum mechanical (QM) density functional theory (DFT) calculations are combined with molecular mechanics (MM). The QM/MM method has emerged as a powerful tool for understanding and predicting both enantioselectivity and regioselectivity in several catalytic systems.[41−46] The systems studied here are rather rigid. Thus it is not likely that one in general will have to consider a Boltzmann distribution of several conformational isomers for the different species under investigation

The present computational study was based on density functional theory using the Becke−Perdew exchange−correlation functional[47−49] as implemented in the Amsterdam density functional (ADF) program.[50] A double-ξ STO basis with one set of polarization functions was used to describe all atoms except palladium, for which a triple-ξ STO basis set was used.[51] The 1s electrons of C and O, the 1s−2p electrons of P, and the 1s−3d electrons of Pd were treated as frozen core. All the reported energy differences include a first-order scalar relativistic correction,[52−54] which has been shown to be sufficient for 4d transition metal atoms.[55] All the reported stationary points were fully optimized in the gas phase without imposing geometrical restrictions. However, relativistic effects were not taken into account for the geometries, and no attempt was made to characterize stationary points from a frequency analysis. Furthermore, the conductor-like screening model (COSMO),[56−58] as implemented in ADF,[59] was employed in order to introduce solvent effects. All the energies in the text were obtained from single-point calculations on the gas-phase-optimized structures, considering toluene as the solvent. Possible exceptions from the choice of procedures described above will be discussed later to the extent that they occur.

Results and Discussion

The optimized structures of the reaction intermediates and the transition states involved in the first olefin insertion step are represented in Figure 1. The relative energies of these structures are listed in Table 1. The structures and the energies of the stationary points located along the second olefin insertion pathway are summarized in Figures 3 and 4 and in Table 2. The relative energies of all the stationary points located along the migratory insertion pathways are represented in Figure 2. The optimized structures for the β-elimination reaction are collected in Figure 5. The relative energies of these stationary points are summarized in Table 3 and Figure 6. In the following we will first discuss the 6-exo and 7-endo routes in the first olefin insertion, then the 4-exo, 5-endo, 5-exo, and 6-endo routes in the second olefin insertion, and finally, the β-elimination in the corresponding 6-exo, 7-endo, 5-exo, and 6-endo intermediates.

a. First Olefin Insertion. All the possible reaction intermediates and transition states involved in the first

(38) Balcells, D.; Maseras, F.; Lledós, A. *J. Org. Chem.* **2003**, *68*, 4265.
(39) Michalak, A.; Ziegler, T. *J. Am. Chem. Soc.* **2001**, *123*, 12266.
(40) *Computational Modeling of Homogeneous Catalysis*; Maseras, F., Lledós, A., Eds.; Kluwer: Dordrecht, 2002.
(41) Deng, L.; Ziegler, T.; Woo, T.; Margl, P. M.; Fan, L. *Organometallics* **1998**, *17*, 3240.
(42) Woo, T. K.; Ziegler, T. *J. Organomet. Chem.* **1999**, *591*, 204.
(43) Deng, L.; Margl, P.; Ziegler, T. *J. Am. Chem. Soc.* **1999**, *121*, 6479.
(44) Ujaque, G.; Maseras, F.; Lledós, A. *J. Am. Chem. Soc.* **1999**, *121*, 1317.
(45) Vázquez, J.; Pericàs, M. A.; Maseras, F.; Lledós, A. *J. Org. Chem.* **2000**, *65*, 7303.
(46) Carbó, J. J.; Maseras, F.; Bo, C.; van Leeuwen, P. W. N. M. *J. Am. Chem. Soc.* **2001**, *123*, 7630.
(47) Becke, A. *Phys. Rev. A* **1988**, *38*, 3098.
(48) Perdew, J. P. *Phys. Rev. B* **1986**, *34*, 7406.
(49) Perdew, J. P. *Phys. Rev. B* **1986**, *33*, 8822.
(50) TeVelde, G.; Bickelhaupt, F. M.; Baerends, E. J.; Fonseca Guerra, C.; Van Gisbergen, S. J. A.; Snijders, J. G.; Ziegler, T. *J. Comput. Chem.* **2001**, *22*, 931.
(51) Snijders, J. G.; Baerends, E. J.; Vernoijs, P. *At. Nucl. Data Tables* **1982**, *26*, 483.
(52) Ziegler, T.; Tschinke, V.; Baerends, E. J.; Snijders, J. G.; Ravenek, W. *J. Phys. Chem.* **1989**, *93*, 3050.
(53) Snijders, J. G.; Baerends, E. J. *J. Mol. Phys.* **1978**, *36*, 1789.
(54) Snijders, J. G.; Baerends, E. J.; Ros, P. *Mol. Phys.* **1979**, *38*, 1909.
(55) Deng, L.; Ziegler, T.; Woo, T. K.; Margl, P.; Fan, T. *Organometallics* **1998**, *17*, 3240.
(56) Pascual-Ahuir, J. L.; Silla, E.; Tomasi, J.; Bonaccorsi, R. *J. Comput. Chem.* **1987**, *8*, 778.
(57) Klamt, A.; Schüürmann, G. *J. Chem. Soc., Perkin Trans.* **1993**, *2*, 799.
(58) Klamt, A. *J. Phys. Chem.* **1995**, *99*, 2224.
(59) Pye, C. C.; Ziegler, T. *Theor. Chem. Acc.* **1999**, *101*, 396.

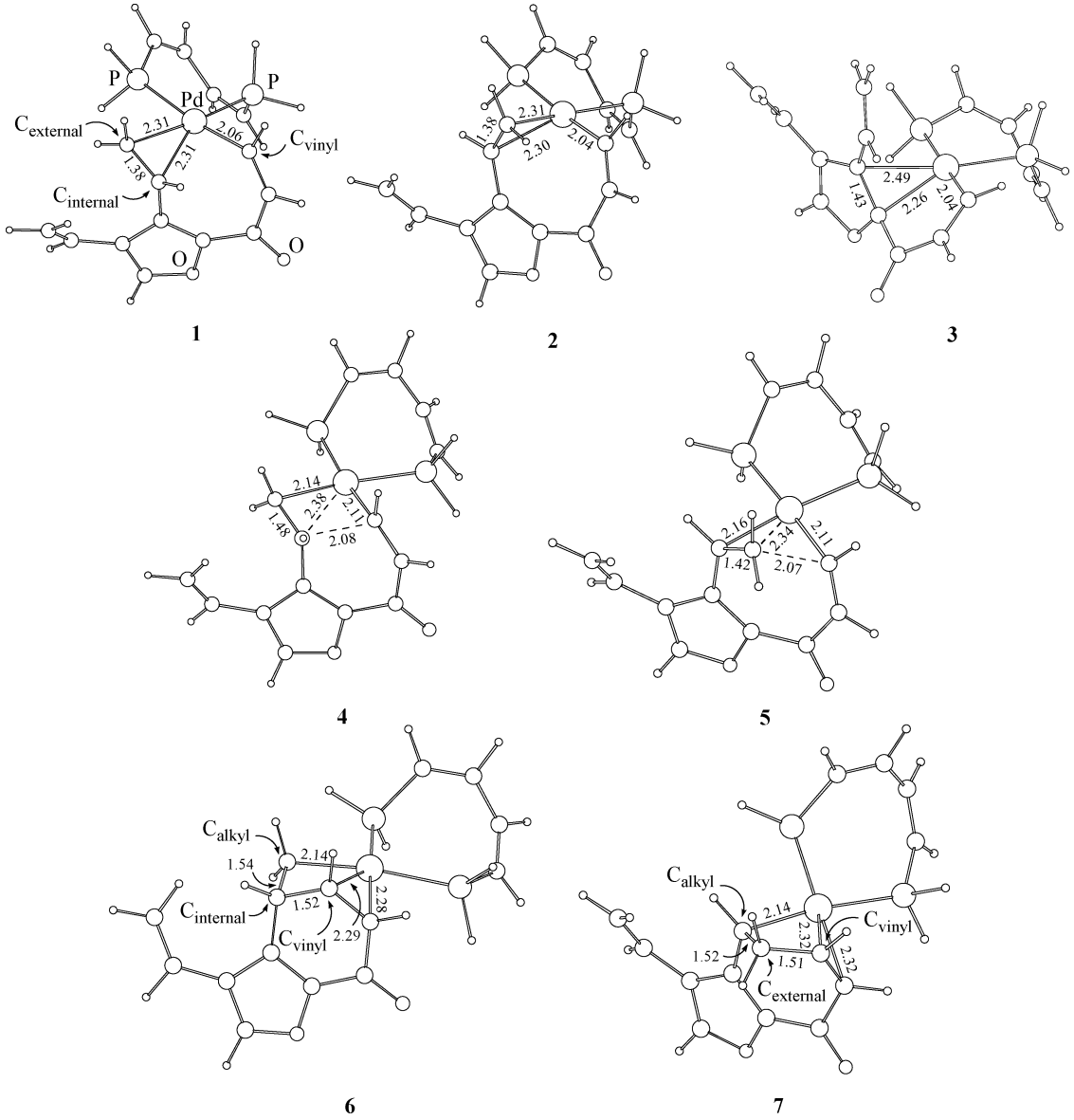

Figure 1. Stationary points located along the first migratory insertion pathway. All the interatomic distances are in Å. The heteroatoms are indicated in complex **1**.

Table 1. Relative Energies, in kcal/mol, of the Stationary Points Involved in the First Olefin Insertion

	gas phase	toluene	NMP
1	0.0	0.00	0.0
2	+1.2	+0.2	+0.0
3	+2.7	+2.4	+2.7
4	+4.7	+4.1	+4.5
5	+9.4	+9.4	+10.0
6	−23.2	−23.8	−23.0
7	−22.7	−22.7	−22.4

Table 2. Energies Relative to 1, in kcal/mol, of the Stationary Points Involved in the Second Olefin Insertion

	gas phase	toluene
8	−12.7	−16.8
9	−22.0	−25.1
10	−19.0	−17.6
11	+12.4	+9.6
12	−0.0	−2.3
13	−14.7	−14.0
14	−46.2	−46.6
15	−8.9	−10.7
16	−12.0	−14.3
17	−29.3	−28.5
18	+47.4	+46.1
19	+25.4	+24.5
20	+23.4	+23.4
21	−30.9	−30.9

olefin insertion step were located on the potential energy surface, for both the exo and the endo pathways. The π-complexes **1** and **2** were found to undergo a migratory insertion, yielding the complexes **6** and **7** through the transition states **4** and **5**, respectively (see Figure 1). Complex **1** has the olefinic bond in the palladium coordination plane, whereas the olefinic bond in **2** has an out-of-plane orientation. In **1** the dihedral angle (*D*) formed between the Pd−P vector trans to the Pd−C σ-bond and the olefinic linkage is −36.9° compared to a value of −121.1° for the same angle in **2**. The two conformers can be interconverted by a 180° rotation of the olefinic unit around its σ-bond to the furan ring.

If **1** and **2** react to form a six-membered ring, then the substituted olefin carbon becomes a chiral center with a different absolute configuration in each case.

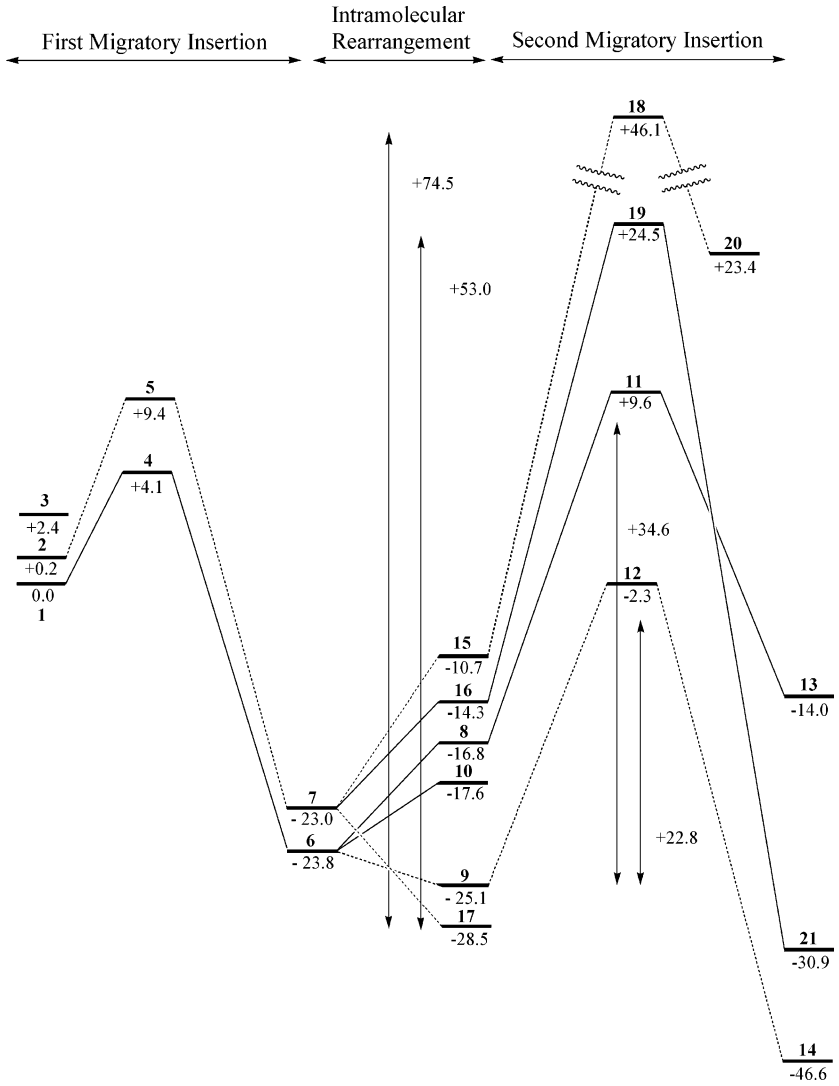

Figure 2. Relative energy profiles for the two sequential olefin insertions. The solid line is for the exo route, while the dotted line is for the endo. All the energies are in kcal/mol.

Table 3. Energies Relative to 1, in kcal/mol, of the Stationary Points Involved in the First and Second β-Eliminations

	gas phase	toluene
22	−5.5	−8.2
23	−6.6	−9.0
24	−13.0	−13.6
25	−12.0	−13.0
26	−13.1	−13.7
27	−6.0	−8.7
28	−4.1	−6.4
29	−26.7	−29.6
30	−17.5	−20.9
31	−19.2	−21.6

Nevertheless, in the π-complex **1** the vinyl carbon bound to palladium is clearly closer to the substituted (internal, see **1**) olefin carbon (2.69 Å) than to the unsubstituted (external, see **1**) carbon (3.43 Å), while in **2** the opposite is the case (3.26 and 2.76 Å, respectively). Thus, the migratory insertion from **1** follows the exo pathway, yielding a six-membered ring (6-exo route), while **2** gives rise to the endo pathway, yielding a seven-membered ring (7-endo route). All attempts to locate an endo transition state directly connected to **1** converged to **4**, while any search for an exo transition state connected to **2** always converged to **5**. Therefore, it seems that in this intramolecular catalytic system the orientation of the olefinic bond relative to the palladium coordination plane controls the exo/endo character of the migratory insertion instead of the absolute configuration of the chiral carbon resulting from the insertion.

The π-complex **1** has a square-planar geometry as expected for a four-coordinated Pd(II) complex.[60] In fact, the square-planar arrangement has been observed for all the optimized stationary points, as the d^8-configuration is preserved along all the explored reaction pathways. The computed energies (see Table 1 and Figure 2) show that **1** is slightly more stable than **2**, by 0.2 kcal/mol. Thus, there is not a clear preference for an out-of-plane olefin coordination in this system, as has been observed for some palladium-based olefin polymerization catalysts.[39,61,62]

We have also examined a complex in which one of the delocalized π-bonds of the furan ring is bound to palladium. The complex **3** has an energy that is only slightly higher than **1** (by 2.4 kcal/mol) and **2** (by 2.1

(60) Albright, T. A.; Burdett, J. K.; Whanbgo, M. H. *Orbital Interactions in Chemistry*; John Wiley & Sons: New York, 1985.
(61) Deng, L.; Margl, P.; Ziegler, T. *J. Am. Chem. Soc.* **1997**, *119*, 1094.
(62) Michalak, A.; Ziegler, T. *Organometallics* **1999**, *18*, 3998.

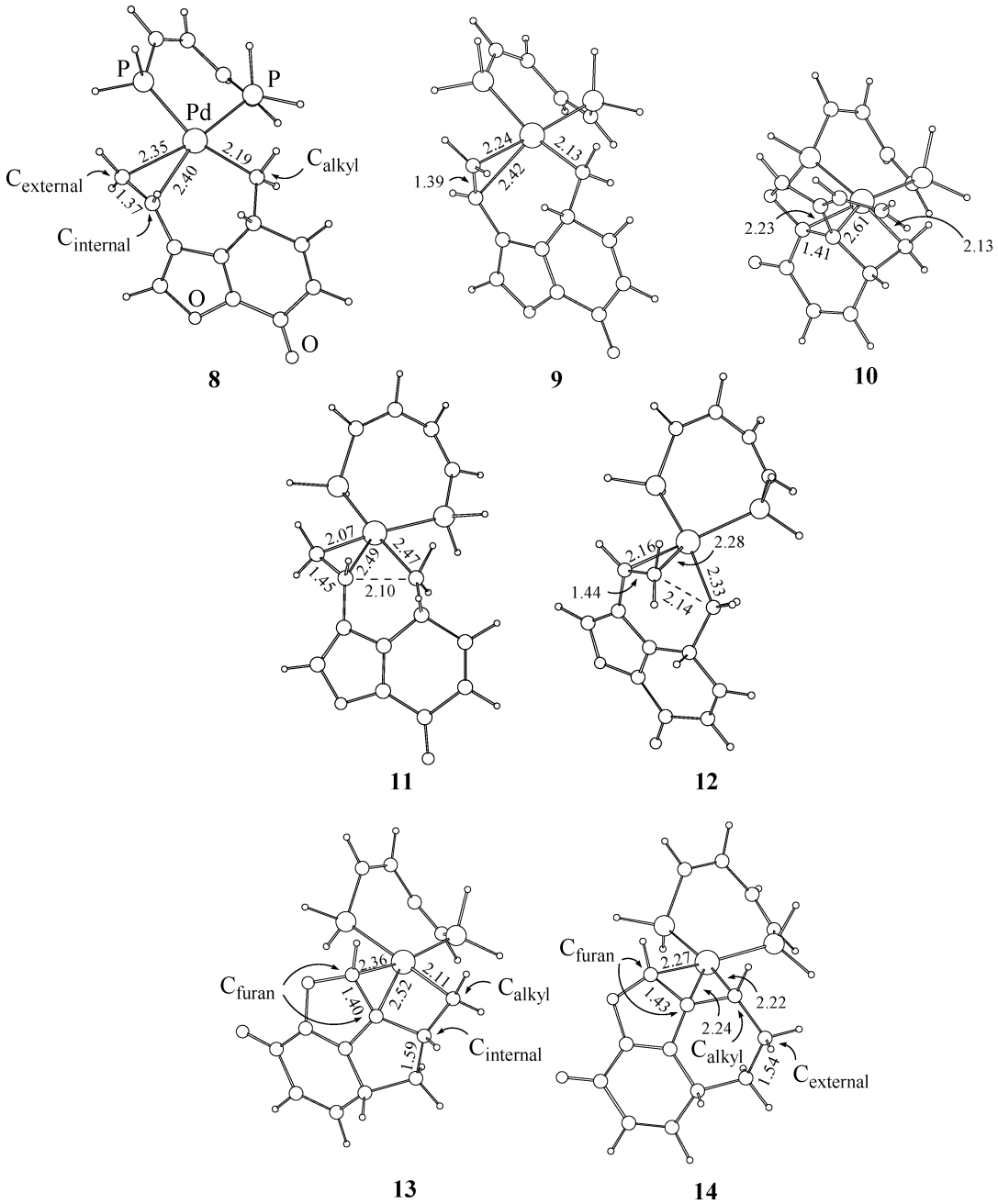

Figure 3. Stationary points involved in the second migratory pathway in the 6-exo intermediate. All the interatomic distances are in Å. The heteroatoms are indicated in complex **8**.

kcal/mol), Table 1. Nevertheless, an olefin insertion from this complex will yield a strained four-membered ring and break the furan aromaticity at the same time. Therefore, such an insertion is very unlikely to happen. In fact, no reaction product derived from a migratory insertion involving the furan ring has ever been observed. Thus, we shall not consider insertion from **3** any further.

The transition states **4** and **5** correspond to the 6-exo and 7-endo insertion pathways, respectively (see Figure 1). The potential energy barrier for the 6-exo olefin insertion is only 4.1 kcal/mol (see Figure 2). In the structure of the transition state **4** we observe the emergence of bonds between $C_{internal}$ and C_{vinyl} (2.08 Å) as well as between Pd and $C_{external}$ (2.14 Å), coupled with the elongation of the olefin linkage (1.48 Å) and the bond between Pd and C_{vinyl} (2.11 Å). All these changes are typical of a (exo) migratory insertion in which a new (six-membered) ring is formed. Equivalent structural features characterize transition state **5** in which a seven-membered ring is assembled (see Figure 1). The energy barrier of 9.4 kcal/mol (see Figure 2) for the 7-endo olfefin insertion is clearly higher than the barrier for the 6-exo route. Hence, the 6-exo insertion is kinetically favored over the 7-endo insertion. The calculated Pd−vinyl insertion barriers are clearly lower than those found[62] for insertion into Pd−alkyl bonds (∼20 kcal/mol).

The exo pathway (**1** → **4**) leads to the insertion product **6** with a new six-membered ring, whereas the endo pathway (**2** → **5**) affords the insertion product with a seven-membered ring. The exo migratory insertion gives rise to the new Pd−$C_{external}$ (2.14 Å) and $C_{internal}$−C_{vinyl} (1.52 Å) bonds in **6**. The palladium atom is in

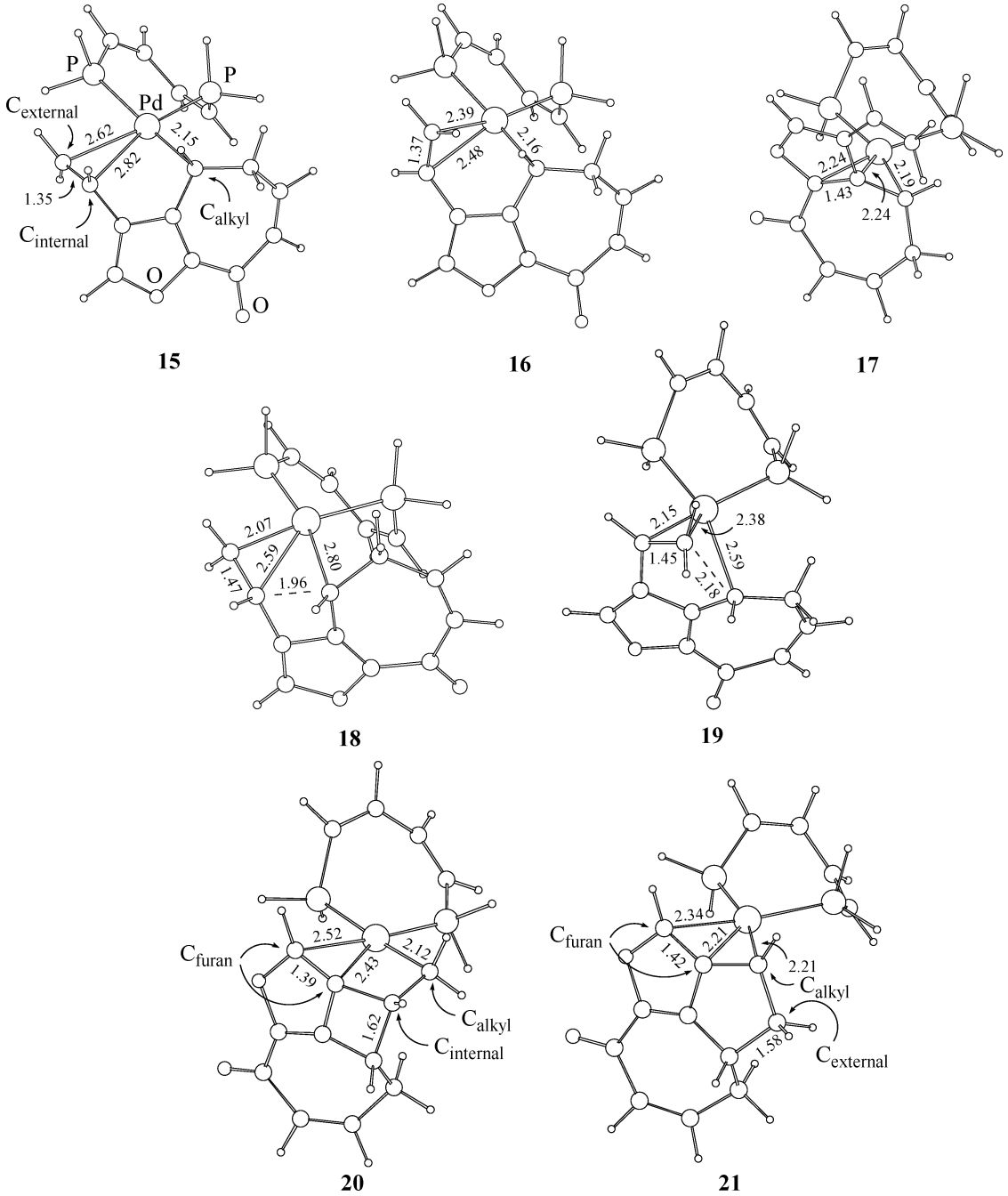

Figure 4. Stationary points involved in the second migratory pathway in the 7-endo intermediate. All the interatomic distances are in Å. The heteroatoms are indicated in complex **15**.

addition π-bonded (R(Pd−olefin) = 2.29 and 2.28 Å) to the olefin modeling the phenyl ring of the real substrate (see Scheme 4). The endo product **7**, with the seven-membered ring, is also seen to gain extra stability through a π-bond between palladium and a conjugated double bond in the newly formed seven-membered ring. The computed relative energies (see Table 1 and Figure 2) show that the first migratory insertion is clearly exothermic, with a ΔE of −23.8 kcal/mol and −23.0 kcal/mol for the 6-exo and 7-endo routes, respectively.

The primary product observed experimentally[36] from the first insertion is the six-membered ring **6**. The computed energy profile for the first olefin insertion step (see Figure 2) indicates the 6-exo route is kinetically favored over the 7-endo pathway by a significant energy difference of 5.2 kcal/mol. The exo route is the reaction path most often observed experimentally.[63,64] In fact, a stepwise bypass mechanism has been proposed[65−67] for those experimental studies where the endo product was observed.[68] This mechanism consists of two exo insertion steps followed by an isomerization reaction and a final β-elimination step affording the endo reaction product.

Nevertheless, for the case at hand the complexes found along the 7-endo route are almost as stable as

(63) Thorn, D. L.; Hoffmann, R. *J. Am. Chem. Soc.* **1978**, *100*, 2079.
(64) Gibson, S. E.; Guillo, N.; Middleton, R. J.; Thuilliez, A.; Tozer, M. J. *J. Chem. Soc., Perrkin Trans. 1* **1997**, 447.
(65) Rawal, V. H.; Michoud, C. *J. Org. Chem.* **1993**, *58*, 5583.
(66) Owczarczyk, Z.; Lamaty, F.; Vawter, E. J.; Negishi, E. I. *J. Am. Chem. Soc.* **1992**, *114*, 10091.
(67) Albeniz, A. C.; Espinet, P.; Lin, Y. S. *J. Am. Chem. Soc.* **1996**, *118*, 7145.
(68) Rigby, J. H.; Hughes, R. C.; Heeg, M. J. *J. Am. Chem. Soc.* **1995**, *117*, 7834.

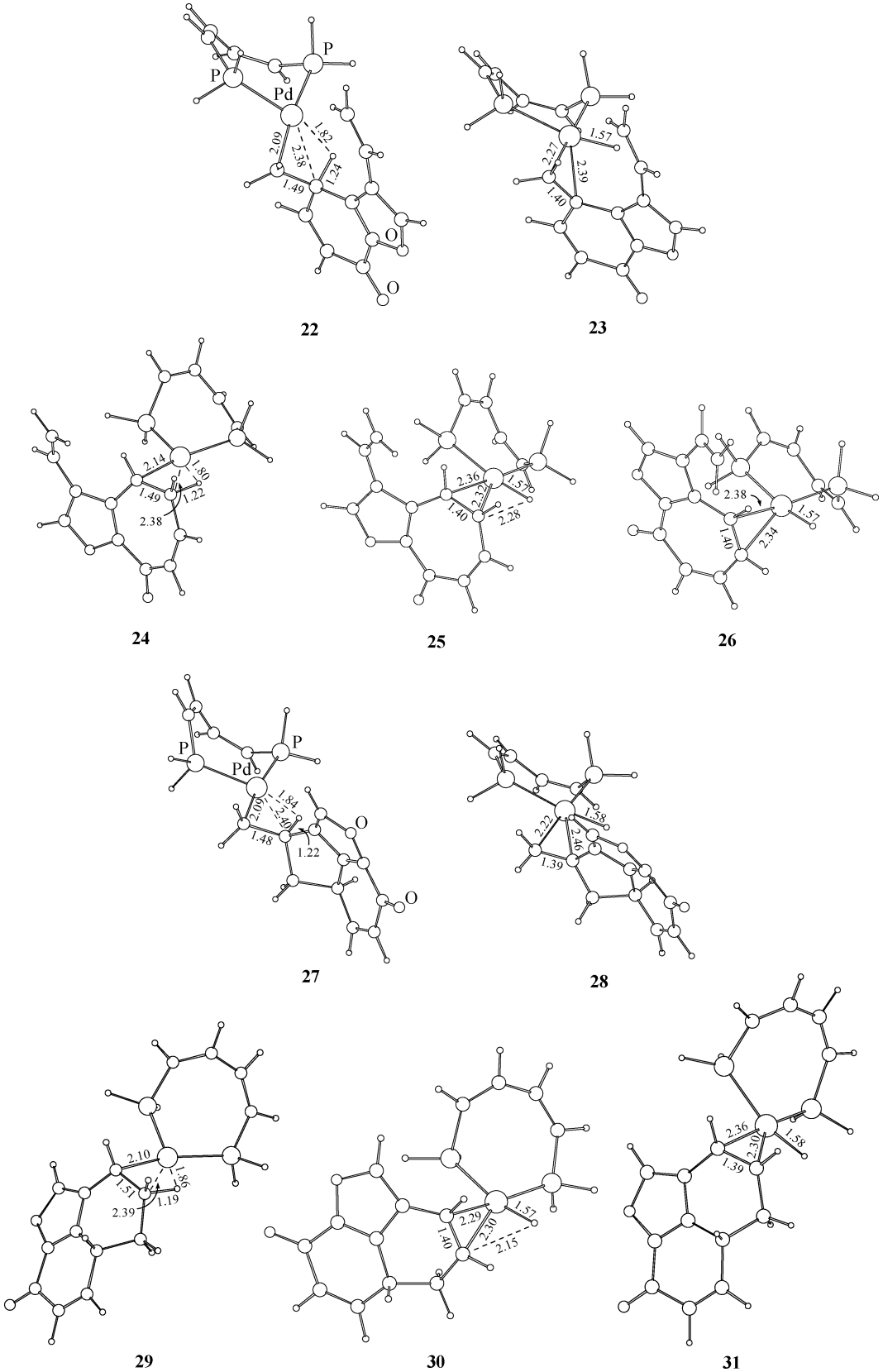

Figure 5. Stationary points involved in the first and second β-eliminations. All the interatomic distances are in Å. The heteroatoms are indicated in complexes **22** and **27**.

those located along the 6-exo path, Figure 2 and Table 1. Hence, the formation of the seven-membered ring should be possible from the thermodynamic point of view at sufficiently high temperatures. In fact, by changing from the less polar solvent toluene ($\epsilon = 2.38$) at a reaction reflux temperature of 383 K to the more polar NMP ($\epsilon = 32.0$) solvent at a reaction reflux temperature of 475 K, Keay et al.[36] observed a reaction product resulting from a β-elimination in the 7-endo intermediate **7**; see **D** → **E** of Scheme 3. According to

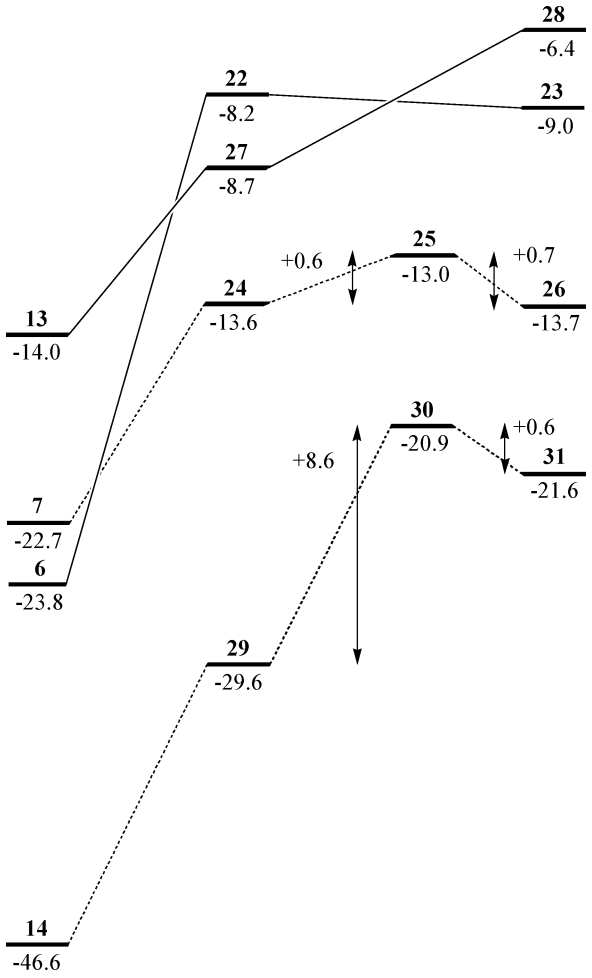

Figure 6. Relative energy profiles for the β-eliminations. The solid line is for the exo route, while the dotted line is for the endo. All the energies are in kcal/mol.

our calculations, when the polarity of the solvent is increased by changing toluene ($\epsilon = 2.38$) for NMP ($\epsilon = 32.0$), the energy differences between **1** and **2** and between **6** and **7** are lowered from 0.2 to 0.0 and from 0.8 to 0.6 kcal/mol, respectively. Furthermore, assuming a Boltzmann thermal population yields at 475 K a **6**:**7** ratio of 1.9:1, very close to the experimentally[36] observed **I**:**E** ratio of 2.5:1.

b. Double Heck Reaction Mechanism. Second Olefin Insertion in the 6-exo Intermediate. All the stationary points along the second olefin insertion pathway starting from the 6-exo product **6** (see Figure 1) have been computed, for both the exo and the endo routes. An intramolecular rearrangement of the reaction intermediate **6** leads to the formation of the π-complex **8** (see Figure 3). The structure of **8** is characterized by the Pd−C_{alkyl} linkage (2.19 Å) formed in the first olefin insertion and a Pd−olefin bond ($C_{external}-C_{internal} = 1.37$ Å); see Figure 3. The same structural features can be observed in the π-complex **9** (see Figure 3). The main difference between **8** and **9** is the position of the coordinated olefin relative to the PPdP catalyst plane. In **8** the olefin takes on an in-plane position ($D = 15.4°$), whereas the orientation is out-of-plane in **9** ($D = -84.9°$). The perpendicular orientation is favored by 8.2 kcal/mol; see Table 2 and Figure 2.

A rotation of the σ-bond connecting the palladium-coordinated olefin to the furan ring provides a facile route for the interconversion between the conformations **8** and **9**. In the intermediate **8** (see Figure 3) the alkyl carbon bound to palladium is clearly closer to the internal olefin carbon (3.07 Å) than to the external (3.87 Å), while in complex **9** we observed the opposite situation (3.31 and 3.16 Å, respectively). Hence, as in the first migratory insertion described in the previous section, **8** and **9** undergo 5-exo and 6-endo insertions, respectively. Therefore, the rotation of the σ-bond between the olefin and the furan ring determines the exo/endo regioselectivity.

One more possible conformation of the cationic palladium complex **8** is the reaction intermediate **10** (see Figure 3). In this π-complex, the furan ring of the substrate is bound to palladium with the Pd−C_{furan} bond distances of 2.23 and 2.61 Å, respectively. As we discussed in the previous section, such a complex is inert and therefore capable of blocking the reaction. In fact, this complex is 7.4 kcal/mol less stable than **9** but 0.8 kcal/mol more stable than **8** (see Table 2 and Figure 2). Hence, the coordination of the furan ring yielding the π-complex **10** can play an important role in hampering the 5-exo route. Taking into account these results, we can infer that the 6-endo insertion is favored over the 5-exo insertion from the thermodynamic point of view due to the formation of the stable π-complex **9**.

A migratory olefin insertion involving **8** and **9** leads to the formation of the reaction intermediates **13** and **14** through the transition states **11** and **12**, respectively (see Figure 3). The transition state **11** exhibits a weakening of the Pd−C_{alkyl} interaction (2.47 Å) and an emerging $C_{internal}-C_{alkyl}$ bond (2.10 Å). With the new $C_{internal}-C_{alkyl}$ bond, a five-membered ring is assembled, while the olefin unit is elongated (1.45 Å) and a new Pd−$C_{external}$ linkage (2.07 Å) is being established. The same structural features can be observed in the 6-endo transition state **12**, with the main difference being the size of the assembled cycle, which now is a six-membered ring.

Two other significant structural differences between **11** and **12** are the relative position of the inserted olefin and the internal conformation of the substrate. In **11** the inserted olefin is close to the parallel position ($D = 9.6°$) with respect to the PPdP catalyst plane, which should be more favorable for a four-center transition, whereas the orientation in **12** is out-of-plane ($D = -142.7°$). On the other hand, in **11** the substate is in a more open and less strained conformation than in **12**. Overall, the 6-endo saddle point **12** is calculated to be 11.9 kcal/mol more stable than the 5-exo transition state **11**, Figure 2 and Table 2. Considering the calculated energy barriers (relative to **9**) of 22.8 kcal/mol for the endo route and 34.6 kcal/mol for the exo route (see Figure 2) we can state that the 6-endo insertion is kinetically preferred over the 5-exo route.

The energy relaxation of the transition states **11** and **12** leads to the π-complexes **13** and **14**, respectively (see Figure 3). In **13** we notice a new Pd−C_{alkyl} (2.110 Å) link and the formation of a C−C bond (1.585 Å) to close the five-membered ring. Furthermore, the reaction intermediate **13** is stabilized by a π-interaction between the aromatic furan ring of the substrate and the metal (R(Pd−C_{furan}) = 2.36 and 2.52 Å). In the π-complex **14** (see Figure 3), resulting from the 6-endo insertion, the

$Pd-C_{alkyl}$ (2.22 Å) linkage is longer and the $Pd-\pi$ (furan) bonds shorter (2.22, 2.27 Å). The computed relative energies indicate that **13** is 32.6 kcal/mol less stable than **14**. This large energy difference is primarily due to the high strain developed in the 6,5,5-membered polycyclic system of **13**. The ring strain is likely to play an important role also in the energy splitting between the transition states **11** and **12**.

Taking into account all the computed relative energies, we can conclude that the 6-endo route is both thermodynamically and kinetically favored over the 5-exo route in the second olefin insertion from the 6-exo intermediate **6** due to a less severe ring strain. Further, the DFT calculations on this model system reproduce the experimentally observed inversion of the regioselectivity from exo in the first insertion to endo in the second. We shall in section **e** discuss how the favored product **14** can undergo a final β-elimination to produce **31** and the primary product modeling **I** (see Schemes 3 and 4).

c. Double Heck Reaction Mechanism. Second Olefin Insertion in the 7-endo Intermediate. The second olefin insertion from the 7-endo reaction intermediate **7** (see Figure 1) was also explored. The reaction pathways **15** → [**18**]‡ → **20** and **16** → [**19**]‡ → **21** were computed for the 4-exo and 5-endo routes, respectively (see Figure 4). Here, the π-complexes **15** and **16** result from an intramolecular rearrangement of the reaction intermediate **7**. The π-complexes **15** and **16** undergoing the insertion are as in the previously described intramolecular migratory insertions distinct conformations linked by the rotation of the σ-bond connecting the activated olefin to the furan ring. Again, this σ-bond rotation controls the exo/endo regioselectivity as the $C_{external}-C_{alkyl}$ (3.65 Å in **15** and 3.00 Å in **16**) and $C_{internal}-C_{alkyl}$ (2.94 Å in **15** and 3.01 Å in **16**) distances point out.

Furthermore, in **16**, which is 3.5 kcal/mol more stable than **15** (see Table 2 and Figure 2), the olefin is almost perpendicular to the PPdP catalyst plane ($D = -86.8°$), while in **15** it is closer to the parallel position ($D = 15.2°$). Thus, as in the second olefin insertion from the 6-exo intermediate, the system prefers a perpendicular coordination of the olefin with a stronger $Pd-C_{external}$ interaction. An intramolecular rearrangement of **15** or **16** can further lead to the formation of the inert π-complex **17**, in which the furan cycle is bound to palladium. This unproductive and inert complex, which is 17.8 and 14.2 kcal/mol more stable than **15** and **16**, respectively (see Table 2 and Figure 2), will constitute the resting state for the second insertion starting from **7**.

The 4-exo insertion process **15** → [**18**]‡ → **20** has a barrier of 74.5 kcal/mol (relative to **17**) and leads to the product **20** with a new four-membered ring, Figure 2. The strain in the new ring and the rest of the conjugated structure is responsible for the high barrier and the substantial (51.9 kcal/mol) endothermicity of the reaction, Figure 2. The alternative 5-endo insertion process **16** → [**19**]‡ → **21** also has a high barrier (53.0 kcal/mol) but is slightly exothermic (−2.4 kcal/mol). It is clear from our calculations that a second insertion starting from the product **7** due to the first 7-endo insertion path is unlikely to take place. In fact, products from such insertion paths have never been observed experimentally.[36] Instead it is likely that **7** undergoes a β-elimination process similar to the reaction **D** → **E** + $PdHL_2^+$ of Scheme 3. Here **E** is an observed side product at higher temperatures in polar solvents.[36] This possibility will be discussed in the next section.

d. Common (Single Insertion) Heck Reaction Mechanism. First β-Elimination. The common Heck reaction mechanism consists of a single olefin insertion followed by a final β-elimination step affording the reaction product. All the mechanistic details about the first migratory insertion step have been discussed in section **a**, and we shall now proceed to discuss the possible subsequent β-elimination reaction. The β-elimination pathway was explored for both the 6-exo and the 7-endo intermediates. In the former case, the β-elimination is not possible in the experimental system because the β-carbon is bound to a methyl group. Nevertheless, we explored the 6-exo route in order to elucidate whether the β-methyl group is essential for the observed product distribution.

An intramolecular arrangement of the π-complex **6**, resulting from the 6-exo first olefin insertion (see Figure 1), leads to the formation of the β-agostic complex **22** (see Figure 5), which is 15.6 kcal/mol higher in energy than **6**. In the structure of this complex, the elongated $C_\beta-H_\beta$ bond (1.24 Å) and the short $Pd-H_\beta$ distance (1.82 Å) clearly point to a β-agostic interaction between the metal and the $C_\beta-H_\beta$ bond. The same structural features can be observed for the β-agostic complex **24** derived from the 7-endo intermediate **7** (see Figure 1), which is 5.4 kcal/mol more stable than the β-agostic complex **22** (see Table 3 and Figure 6) and 9.4 kcal/mol higher in energy than **7**.

The structure **25** represents the transition state corresponding to the β-elimination reaction starting from **24** (see Figure 5). The $C_\beta-H_\beta$ and $Pd-H_\beta$ bond distances of 2.28 and 1.57 Å, respectively, reflect the rupture of the $C_\beta-H_\beta$ linkage coupled with the formation of the $Pd-H_\beta$ bond. At the same time a Pd-olefin π-complex is formed with $R(Pd-C_\alpha) = 2.36$ Å and $R(Pd-C_\beta) = 2.32$ Å. As in the starting β-agostic complex **24**, the $C_\alpha-C_\beta$ vector in **25** is almost parallel to the PPdP catalyst plane; thus, the dihedral angle $P_{cis}-Pd-C_\alpha-C_\beta$ (DD) is −176.9° in **24** and 172.4° in **25**. The transition state **25** is only 0.6 kcal/mol above the starting β-agostic complex **24** (see Table 3 and Figure 6), and therefore the β-elimination in this system is extremely fast. We were unable to locate a transition state for the β-elimination process **22** → **23** due to the shallow nature of the potential energy surface around this pass. Thermodynamically, the process is exothermic by −0.8 kcal/mol.

The hydride complexes **23** and **26** were optimized as the reaction products of the β-elimination from the complexes **22** and **24**, respectively (see Figure 5). The 7-endo hydride **26** is clearly more stable than the 6-exo hydride **23** by 4.7 kcal/mol (see Table 3 and Figure 6), probably due to the stronger coordination of the more electron-rich olefin present in **26**. The fully characterized 7-endo pathway indicates that the β-elimination on this reaction system is extremely fast and almost isothermic ($\Delta E = -0.1$ kcal/mol; see Table 3 and Figure 6) and therefore should be highly reversible, as it has been found in other computational studies.[12,24]

It follows from the analysis above that the 7-endo insertion product **7** can generate the hydride olefin complex **26** via the β-agostic complex **24** at an energy cost of 9.3 kcal/mol, Figures 2 and 6. The complex **26** can further decompose into the metal hydride $L2PdH^+$ and our model (**E′**) of the cyclic product **E**; see **D** → **E** of Scheme 3. With an olefin dissociation energy of 20.3 kcal/mol the entire process **7** → **E′** + $L2PdH^+$ would require 29.6 kcal/mol on the potential energy surface. On the free energy surface this energy would be reduced by ~15 kcal/mol due to the olefin dissociation. Alternatively **7** could disinsert to regenerate the starting complex **2**, which subsequently could isomerize to **1** and produce **6** by insertion. The energy barrier for **7** → **2** is 32.0 kcal/mol. It is thus likely that the ultimate fate for **7** would be **E′** + $L2PdH^+$. Indeed the product **E** has been observed, as already mentioned. One could also envision that **7** would undergo a second insertion. However, the barrier for this process is prohibitively high (>50 kcal/mol), as shown in Figure 2.

The corresponding β-elimination process involving the 6-exo insertion product **6** (**6** → **22** → **23**) is only slightly more endothermic, with ΔE =14.8 kcal/mol, Figures 2 and 6. It is thus likely that it would decompose into $L2PdH^+$ and a cyclic product at higher temperatures. In reality such a path is prevented since the β-carbon in the real system (**C** of Scheme 3) modeled by **6** is bound to a methyl group. Instead **6** can undergo a second insertion with a barrier of 22.8 kcal/mol to propagate chemical change, or it could less likely revert to **1** with a barrier of 27.9 kcal/mol, Figure 2. We shall discuss the final stage of the first process in the next section.

e. Second β-Elimination. Double Heck Reaction Mechanism. The β-elimination pathway was also explored for both the 5-exo and 6-endo intermediates resulting from the second olefin insertion, to compare the results to those obtained in the last section from the β-elimination of the 6-exo and 7-endo intermediates due to the first insertion. The β-eliminations of the 4-exo and 5-endo insertion products were not considered since these insertion products are kinetically unfavorable.

An intramolecular rearrangement of the π-complexes **13** and **14** (see Figure 3) leads to the formation of the β-agostic complexes **27** and **29** (see Figure 5). In both complexes we found a β-agostic interaction characterized by the elongation of the $C_\beta-H_\beta$ bond (1.22 Å in **27**) coupled by the shortening of the $Pd-H_\beta$ intramolecular distance (1.84 Å in **27**). From the structural point of view, the agostic interaction is weaker in **29**, as the shorter $C_\beta-H_\beta$ and longer $Pd-H_\beta$ bond distances of 1.19 and 1.86 Å, respectively, indicate. Nevertheless, the β-agostic complex **29** is more stable than **27** by 20.9 kcal/mol (see Table 3 and Figure 6) due to the low stability of the 6,5,5-membered polycyclic structure of **27**.

The species **30** represents the transition state for the β-elimination in the endo β-agostic complex **29** (see Figure 5). The structure of this saddle point reflects the rupture of the $C_\beta-H_\beta$ bond (2.15 Å) and the formation of the $Pd-H_\beta$ linkage (1.57 Å). Furthermore, the shortening of the $C_\alpha-C_\beta$ and $Pd-C_\beta$ bond distances to 1.40 and 2.30 Å, respectively, points to the formation of a $C_\alpha=C_\beta$ double bond coordinated to palladium. The transition state **30** connects the reactant **29** with the β-elimination hydride product **31** (see Figure 5). In this complex a Pd−H bond has formed (1.58 Å), and the olefin resulting from the β-elimination is coordinated to palladium with $Pd-C_\alpha$ and $Pd-C_\beta$ bond distances of 2.36 and 2.30 Å, respectively. Moreover, **30** is only 0.6 kcal/mol above **31** (see Table 3 and Figure 6). Hence, as in the first β-elimination reaction described in the previous section, the transition state and the hydride are almost identical from the energetic and structural points of view; that is, the potential energy surface varies very little in the region connecting **29** with **31**. Also, as in the first β-elimination, an important component of the reaction is the rotation of the $C_\alpha-C_\beta$ bond with respect to the PPdP catalyst plane from a parallel position in **29** (DD = −166.4°) to a perpendicular position in **31** (DD = 126.4°).

Due to the shallow nature of the potential energy surface, all attempts to locate the saddle point for the β-elimination in the exo β-agostic complex **27** failed. The resulting hydride product **28** is 15.1 kcal/mol less stable than the endo hydride (see Table 3 and Figure 6) due to the high intramolecular strain of the 6,5,5-membered polycyclic system.

We have shown that the most stable double-insertion product **14** can rearrange to the β-agostic complex **29** at a cost in energy of 17.0 kcal/mol. Further, **29** can undergo β-hydrogen elimination to produce the most stable hydrido olefin complex **31** with a barrier of 8.6 kcal/mol and a reaction energy of 8.0 kcal/mol. From **31** dissociation is possible into **I′** and $L2PdH^+$ at a cost of 22.9 kcal/mol, Figures 2 and 6. Here **I′** is our model of the primary product **I** observed by Keay et al.[36] Thus the overall conversion **1** → [**4**]‡ → **6** → **9** → [**12**]‡ → **14** → **29** → [**30**]‡ → **31** → **I′** will have a reaction enthalpy of 1.3 kcal/mol. On the free energy surface this reaction would be even less costly by ~15 kcal/mol due to the dissociation of **31** yielding **I′** and $L2PdH^+$. The highest internal barrier for this double Heck reaction would be 22.8 kcal/mol from the second insertion, **9** → [**12**]‡ → **14**.

Conclusions

The first theoretical study of a cascade intramolecular Heck reaction has been presented. The calculations on the first migratory insertion show that the exo route (**1** → [**4**]‡ → **6**) is preferred over the endo path **2** → [**5**]‡ → **7** . Nevertheless, the endo pathway was found to be very close in energy, especially at the thermodynamic level. Furthermore, the energy separation between both routes is reduced as the polarity of the solvent increases. The calculations demonstrated as well that the rotation of the σ-bond connecting the activated olefin to the furan ring of the substrate controls the exo/endo regioselectivity of the first insertion reaction rather than the enantioselectivity.

Any further insertion in the first endo insertion product **7** is kinetically unfavorable, and **7** leads instead via β-hydrogen elimination to **E**, which is observed at higher temperatures as a secondary product.[36] On the other hand, the favored path for the first exo insertion product **6** is to undergo further insertion.

The most favorable second insertion of **6** undergoes a regioselectivity inversion from exo (**1** → [**4**]‡ → **6**), in the first insertion, to endo (**6** → **9** → [**12**]‡ → **14**), in the

second insertion. This exo/endo selectivity inversion is explained by the strain introduced by the rings derived from the second exo insertion (**6** → **8** → [**11**]‡ → **13**). The rings assembled by the exo insertions are always smaller than the rings formed in the endo insertions. The *n*-membered rings with $n \leq 5$ are highly strained. The strain is further amplified when the small ring is formed in the polycyclic environment of the substrate. In fact, the relative stability of the polycyclic system resulting from the migratory insertion is the only general factor ruling the exo/endo regioselectivity in all the possible insertions at both the thermodynamic and kinetic levels. This factor seems to be more important than both the coplanarity in the transition state between the olefin unit and the Pd−C bond and steric interactions favoring the exo insertion arrangement.

The DFT calculations indicate that the second insertion product **14** is the sole product from the double-insertion process based on both kinetic and thermodynamical considerations. The product **14** can subsequently undergo β-hydrogen elimination (**14** → **29** → [**30**]‡ → **31**) to produce the hydrido olefin complex **31**. A final decomposition of **31** results in **I′** and L_2PdH^+, where **I′** models the primary product **I** observed experimentally (Scheme 3). Thus, the present DFT study is able to account for both the secondary (**E**) and the primary (**I**) products observed experimentally. The current model investigation is a first step toward a study of the enantioselectivity of the Heck reaction involving the real system. Such a study is planned by means of the hybrid QM/MM methodology.

Acknowledgment. An important part of the calculations reported here have been performed by the MACI cluster (Multimedia Advanced Computational Infrastructure) at the University of Calgary. This work has been supported by the National Sciences and Engineering Research Council of Canada (NSERC). T.Z. thanks the Canadian government for a Canada Research Chair. D.B. thanks the Catalan DURSI for financing his three month stay at the University of Calgary.

Supporting Information Available: This material is available free of charge via the Internet at http://pubs.acs.org.

OM034310C